Eur. Phys. J. D **31**, 385–393 (2004)
DOI: 10.1140/epjd/e2004-00158-3

THE EUROPEAN PHYSICAL JOURNAL D

Formation of NO(j′ = 7.5) molecules with sub-kelvin translational energy via molecular beam collisions with argon using the technique of molecular cooling by inelastic collisional energy-transfer

M.S. Elioff[1,a], J.J. Valentini[2], and D.W. Chandler[1]

[1] Combustion Research Facility, Sandia National Laboratories, Livermore, CA 94550, USA
[2] Department of Chemistry, Columbia University, New York, NY 10027, USA

Received 1st June 2004
Published online 23 November 2004 –

Abstract. We report the cooling of nitric oxide molecules in a single collision between an argon atom and an NO molecule at collision energies of 5.65 ± 0.36 kJ/mol and 14.7 ± 0.9 kJ/mol in a crossed molecular beam apparatus. We have produced in significant numbers ($\sim 10^8$ molecules cm^{-3} per quantum state) translationally cold NO($^2\Pi_{1/2}$, $v' = 0$, $j' = 7.5$) molecules in a specific quantum state with an upper-limit laboratory-frame rms velocity of 14.8 ± 1.1 m/s, corresponding to a temperature of 406 ± 28 mK. The translational cooling results from the kinematic collapse of the velocity distribution of the NO molecules after collision. Increasing the collision energy by increasing the velocity of the argon atoms, as we do here, does shift the scattering angle at which the cold molecules appear, but does not result in an experimentally measurable change in the velocity spread of the cold NO. This is entirely consistent with our analysis of the kinematics of the scattering which predicts that the velocity spread will actually decrease with increasing argon atom velocity.

PACS. 32.80.Pj Optical cooling of atoms; trapping – 33.80.Ps Optical cooling of molecules; trapping – 34.50.-s Scattering of atoms and molecules

1 Introduction

The interactions of atoms at low temperatures is an appealing, and rapidly growing, field of research. These interactions and their effects distinguish them from the atomic interactions encountered in collisions at ambient temperatures. Recent advances in the methods for the production and trapping of ultracold atoms, with temperatures below 1 μK [1], even less than 1 nK, have brought about the generation of Bose-Einstein condensates [2–4], the observation of atom optics [5], the investigation of collisions at ultra-low energy [6], and the optical clock [7]. Ultracold atoms generally have been prepared in a multistep process. Radiation pressure cooling of atoms, via laser light absorption, yields cold samples ($T < 1$ mK). At sub-millikelvin temperatures, the kinetic energies are low enough to be overcome by potential fields, permitting the cold atoms to be held in a magneto-optical or similar trap, and the temperature further reduced by optical [8,9] or evaporative cooling [10].

Similarly, the study of the properties of molecules at these very low temperatures is a potentially rewarding field of scientific endeavor. Investigators have sought a technique for preparing and containing molecules at nanokelvin-scale temperatures, but have not yet discovered a general method for producing and trapping ultracold molecules [11–13]. Radiation pressure cooling, which is used as the initial step in the trapping of ultra-cold atoms, does not work well for molecules due to their more complex energy-level structures. A few methods have been successful in achieving this first step by producing molecules cold enough to be trapped and further cooled. These methods include photoassociation of ultra-cold atoms [14–17], adiabatic tuning of a Feshbach resonance in a cold atomic gas [18,19], and buffer gas loading [20,21]. Additionally, time-varying inhomogeneous electric fields have been made to produce cold molecules [22]. In particular, Stark deceleration [23] has been shown to be capable of slowing to a stop dipolar molecules which have the appropriate Stark behavior. Another proposed cooling technique is a spinning molecular beam source in which the velocity of the spinning source cancels the velocity of the

[a] e-mail: elioff@sbcglobal.net

molecules flowing through it [24]. These techniques have demonstrated some success in cooling molecules, but each protocol is limited either in its applicability or its implementation.

We recently reported a cooling process for molecules that depends on single collisions between the molecule and an atom in a crossed molecular beam apparatus [25]. This technique was demonstrated to produce NO molecules with a laboratory velocity that is less than 15 m/s. We showed that kinematic analysis indicates that the velocity spread in the cold molecules should depend only on the velocity spread of the NO molecules before the collision, and not on the velocity spread of the molecules with which the NO collides. Herein we report preliminary experimental evidence from our laboratories supporting this prediction.

2 Experimental

The experiments discussed in this paper are performed using a crossed molecular beam velocity-mapped ion imaging apparatus which has been described previously [26,27]. The apparatus is partitioned into two source chambers, two differential pumping chambers, and one scattering chamber. A 4% gaseous mixture of nitric oxide in argon (Matheson) is collided at a 90° angle with a neat argon (Praxair, 99.8%) beam, as shown in Figure 1, as well as with a 12% mixture of argon in helium (Matheson, 99+%). Both molecular beams are produced using a 0.78 mm aperture piezoelectric valve pulsed at a frequency of 30 Hz and propagated through a skimmer and collimator with apertures of 0.60 mm and 0.82 mm, respectively. The source chambers are differentially evacuated using turbomolecular pumps in order to achieve typical base pressures of $\sim 10^{-8}$ Torr with the source valves off and $10^{-4}-10^{-5}$ Torr with the source valves operating at 30 Hz.

Scattered products are probed using $(1+1')$ resonance-enhanced multiphoton ionization (REMPI) detection. The frequency-doubled output of a wavelength-locked Sirah Precision Scan dye laser with Coumarin-450 dye, pumped using an externally triggered Coherent Infinity Nd:YAG laser operating at 30 Hz, provides an excitation beam tunable over $\lambda = 450-454$ nm and doubled for NO($X^2\Pi \rightarrow A^2\Sigma$). This laser beam is propagated perpendicular to the collision plane as illustrated in Figure 1. Ionization is achieved using the 266-nm output of an externally triggered Coherent Infinity XPO, electronically delayed by 5 ns relative to the excitation laser. Master timing is controlled with a SRS 350 digital delay generator. The ionization laser beam, which bisects the intersection angle in the plane of collision, is focused with a lens of focal length 0.52 m through a $\sim$0.8 mm^3 scattering volume between the repeller and extractor ion optics.

Ion imaging is achieved with electrostatic ion extraction lenses [28] arranged perpendicular to the plane formed by the molecular beams. Nitric oxide ions are extracted through an arrangement of ion optics set for velocity mapping conditions [29,30] and accelerated onto a position-sensitive detector which consists of a pair of chevron-type microchannel plates (MCP) and a fast phosphor screen. The phosphorescent images are collected on a cooled charge-coupled device (CCD) camera (Photometrics CH350), and the images are transferred to a computer for analysis. Mass selection of ions is achieved with detection gating by pulsing the front plates of the MCP array with a square-wave voltage of amplitude 400−500 V and a pulsewidth of $\sim$300 ns. In this experimental arrangement, ions of all scattered velocities are sampled and projected onto the two-dimensional detector.

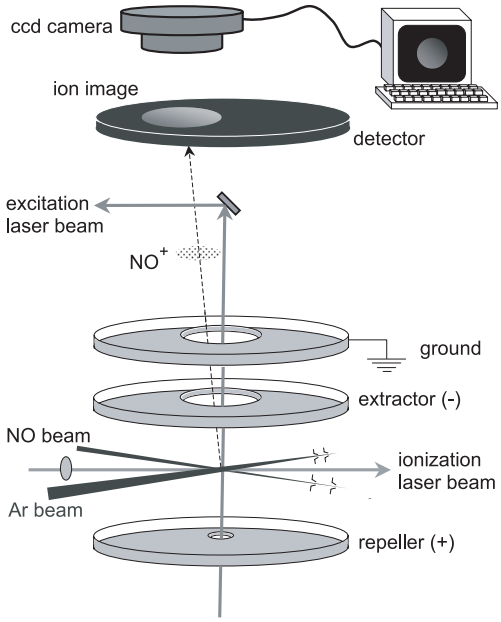

Fig. 1. Crossed molecular beam apparatus diagram depicting the $1+1'$ REMPI probe laser beams and ion imaging arrangement. NO and Ar beams are propagated through two skimmers and intersected at a 90° angle which is bisected by the ionization laser beam. The 226-nm excitation laser beam is directed perpendicular to the scattering plane so as to reduce Doppler broadening due to non-zero velocity distributions in the molecular beams. The ionized NO($^2\Pi$, $j' = 7.5$) scattering products are focused on the position-sensitive detector using velocity-mapped ion optics (repeller and extractor). A pair of chevron type microchannel plates (MCP) and a phosphor screen forms the detection system. A CCD camera is used to collect the two-dimensional projection of the velocity distribution of the scattered product and this raw data is transferred to a computer for analysis.

For probing the NO($j' = 7.5$) rotational state, the $R_{21}(7.5)$ transition at $\lambda = 226.057$ nm is used. Spectral assignments are made using the LIFBASE spectral database and simulation program [31]. Images for NO($j = 0.5$) + Ar $\rightarrow$ NO($j' = 7.5$) + Ar scattering events of interest are acquired as follows: The laser frequency is set to the $Q_{22}(0.5)$ rotational transition for NO($^2\Pi_{1/2}$, $j' = 0.5$) and locked. The NO/Ar gas mixture is supplied to both valves and the pulse timing for each valve is finely tuned to maximize signal in each beam. Maximizing the signal for $j' = 0.5$ ensures that the valve timings are optimized for the coldest, and most intense, part of the molecular beam.

The ionization laser beam is then positioned to propagate through the collision plane and into the center of the interaction volume. The collider beam is then replaced with neat argon and the ion optics are adjusted to velocity mapping voltages. The flight time for NO molecules under these conditions is approximately 8.2 μs. After the ion optics voltages and valve and laser timings have been optimized using the $Q_{22}(0.5)$ transition, the laser frequency is then tuned to the $R_{21}(7.5)$ transition of interest for detection of the scattered NO molecules and the signals are integrated for 30 to 600 seconds, collected on a CCD camera, and saved to a computer for analysis. For background corrections, the activation time of the valve containing the argon collider beam is electronically delayed and a background image is integrated for 30 seconds. Typical signal-to-noise ratios are greater than ten-to-one. Net images are produced by subtracting the background images from the signal images in order to remove intensity due to population of the product rotational state in the uncollided NO/Ar beam, as well as the residual thermal NO in the scattering chamber.

As a verification of our ability to accurately reproduce images for rotational state-specific scattering, we compare our experimentally determined scattering differential cross-section (DCS) with a calculated DCS. The lab frame/center-of-mass frame Jacobian transform typically employed in crossed beam experiments that detect scattering products in the scattering plane [32,33] is not necessary here because ion images are collected parallel to, and above, the scattering plane. Since the lab frame velocity only moves the images onto a different position on the detector, our experimental images represent projections of the center-of-mass scattering distributions of the ionized molecules. The raw data (ion images) are normalized in several ways in order to extract quantitative DCS data from them. Velocity spreads in the molecular beams require that each scattering distribution be modeled as a sum of many discrete scattering spheres, each resulting from a discrete set of molecular beam velocities. Moreover, different scattering velocities are detected by the laser with different efficiencies, therefore DCS extraction involves determination of an apparatus function. This is accomplished by computer simulation of the experimental apparatus, the molecular beam geometry, the laser geometry, and our detection scheme. As described previously [26], the apparatus function is then used to correct the images by dividing an experimental annular intensity pattern by an intensity pattern resulting from a simulated ion image calculated from isotropic scattering. The trial DCS is then iteratively adjusted until the simulated and experimental ion images are equivalent.

Additionally, it is necessary to establish accurately the molecular beam intersection point on the detector, or the origin of the laboratory coordinate system, in order to determine the velocities of the scattered NO molecules. To find the origin, we produce two effusive beams of NO($j = 0.5$), with the mixture of 5% NO in Ar in both pulsed valves and record a velocity-mapped ion image. This image shows two diagonal streaks that mark the two beam propagation axes. Lines are fitted through the streaks and extrapolated to their intersection, which is the origin in the laboratory frame of reference. The angle between the streaks is the intersection angle, which we determine experimentally to be 90.8°.

3 Results

Utilizing two supersonic molecular beams of 5% NO in Ar, we measure the speed of the NO reactant, which we determine to be 592 ± 7 m/s, with a spread of about 9% full-width at half-maximum intensity. The uncertainty in the measurement originates in the resolution of our camera, and the spread reflects the width of the statistical distribution of velocities in the sample of NO molecules. We do not measure the speed of the Ar beam; instead we take the computed value for an ideal isentropic expansion, 556 m/s, and assume a spread of 9% full-width at half-maximum. Previous measurements with pure Ar expansions at these conditions have shown the speed to be within a few percent of the ideal value, with spreads of 5−10%. From these two speeds and the 90.8° intersection angle, we determine a relative collision velocity of 813 ± 52 m/s and a velocity of the center-of-mass of 404 ± 26 m/s, oriented 85.6° with respect to the center-of-mass frame initial NO velocity vector. The computed value for the velocity of the 12% argon seeded in helium is 1187 m/s. From this speed, along with that of the nitric oxide beam, we determine a relative collision velocity of 1320 ± 80 m/s and a velocity of the center-of-mass of 723 ± 46 m/s, oriented at 47.0° with respect to the center-of-mass frame initial NO velocity vector. The collision energies for these two systems are 5.65 ± 0.36 kJ/mol and 14.7 ± 0.9 kJ/mol, respectively.

A scattering DCS is determined, as described above, and shown in Figure 2. Extracted state-resolved differential cross-sections for the inelastic scattering of NO($j = 0.5$) + Ar → NO($j' = 7.5$) + Ar are shown along with those from quantum close-coupling calculations on ab initio coupled-cluster CCSD(T) potential energy surfaces performed using the HIBRIDON 4.1 software [34] for time-independent quantum calculations involving inelastic collisions and photodissociation, and smoothed over a Gaussian angular window of 8° FWHM. The experimental data is shown as a dashed line and the calculated results are shown as a solid line. The DCS data are normalized such that the experimental and calculated plots have equal integrated areas. As can be seen in Figure 2, our extracted DCS is in excellent agreement with the calculated DCS.

False-color images of recoiling NO($^2\Pi_{1/2}$, $v' = 0$, $j' = 7.5$), hereafter denoted $NO_{7.5}$, from NO($j = 0.5$) + Ar → NO($j' = 7.5$) + Ar, are shown in Figure 3. The top left panel of Figure 3 shows $NO_{7.5}$ scattered via collisions occurring between nitric oxide and argon in a neat molecular beam and the bottom left panel shows $NO_{7.5}$ scattered via collisions occurring between nitric oxide and argon in a molecular beam of 12% argon seeded in helium. For the top left image the scattered $NO_{7.5}$ lies on a circle with a radius corresponding to its center-of-mass recoil velocity,

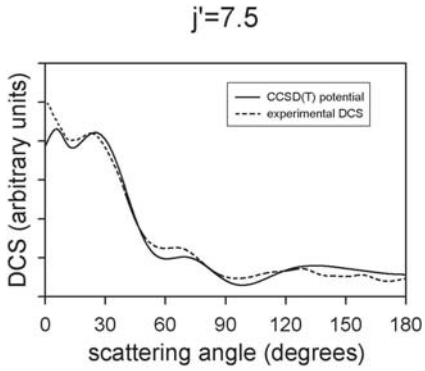

Fig. 2. Extracted state-resolved differential cross-sections for the inelastic scattering of NO($^2\Pi$, $j = 0.5$) + Ar → NO($^2\Pi$, $j' = 7.5$) + Ar, shown along with those from quantum close-coupling calculations on ab initio coupled-cluster CCSD(T) potential energy surfaces performed using the HIBRIDON 4.1 software [34] for time-independent quantum calculations involving inelastic collisions and photodissociation, and smoothed over a Gaussian angular window of 8° FWHM. The experimental data is shown as a dashed line and the calculated results are shown as a solid line. The DCS data are normalized such that the experimental and calculated plots have equal integrated areas.

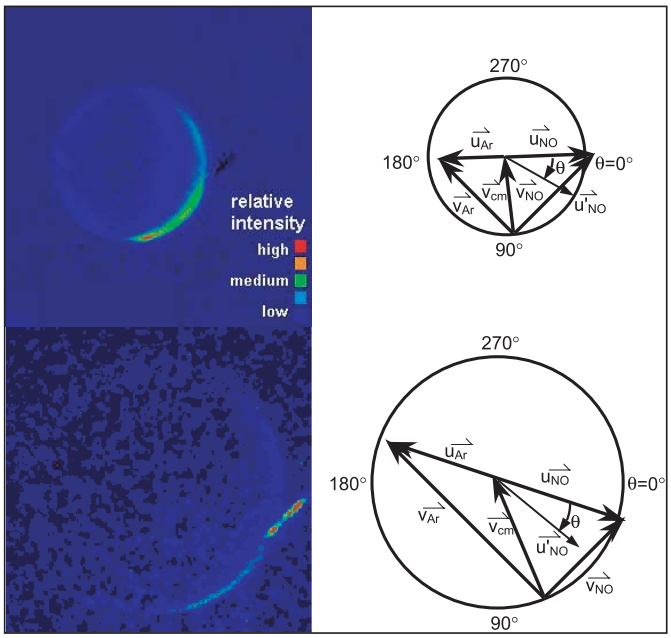

Fig. 3. Typical velocity-mapped ion images for collisions between nitric oxide and argon, NO($^2\Pi_{1/2}$, $j = 0.5$) + Ar → NO($^2\Pi_{1/2}$, $j' = 7.5$) + Ar, shown with the corresponding Newton diagrams. The upper left panel shows a scattering image of $NO_{7.5}$ recoiling from collisions of NO in a beam of 5% NO in Ar with Ar atoms in a beam of pure Ar. This system has a center-of-mass collision energy of 5.65±0.36 kJ/mol. The bright red spot near the bottom of the scattering sphere results from a collapse of the velocity spreads of the molecular beams for those molecules whose scattered velocity vector is equal in magnitude (and opposite in direction) to the center-of-mass velocity of the collision pair. A velocity-mapped ion image for collisions between nitric oxide and argon (12% seeded in helium), NO($^2\Pi_{1/2}$, $j = 0.5$) + Ar → NO($^2\Pi_{1/2}$, $j' = 7.5$) + Ar at a center-of-mass collision energy of 14.7 ± 0.9 kJ/mol is shown in the lower left panel. This scattering sphere is similar to the first image, but it has a larger radius due to the higher collision energy. The right panels show Newton diagrams for inelastic collisions between NO molecules and Ar atoms. Each Newton diagram corresponds to the velocity-mapped scattering image immediately to its left. The lab-frame velocities of the two molecular beams (v_{Ar} and v_{NO}), along with the velocity of the center of mass (v_{cm}) and initial center-of-mass frame velocities of NO and Ar (u_{NO} and u_{Ar}), are shown. Primed and unprimed labels indicate initial and postcollision variables. The molecular beams intersect at an angle of 90.8° and their intersection defines the origin of the laboratory frame of reference. The circle represents the center-of-mass scattering sphere for NO($^2\Pi_{1/2}$, $v' = 0$, $j' = 7.5$).

405 ± 7 m/s, associated with 2.46 ± 0.13 kJ/mol of product translational energy for this state at the total relative collision energy of 5.65 ± 0.36 kJ/mol. The center of the scattering circle is the origin of the center-of-mass coordinate system. This origin is translated with respect to the origin of the laboratory-frame coordinate system, which is the intersection of the NO and Ar beams, by a distance that corresponds to the velocity of the center-of-mass of the NO + Ar system. For the bottom left image the scattered $NO_{7.5}$ lies on a circle with a radius corresponding to its center-of-mass recoil velocity, 722 ± 7 m/s, associated with 7.82 ± 0.31 kJ/mol of product translational energy.

The right panels in Figure 3 show Newton diagrams for the collisions NO with Ar. Each Newton diagram corresponds to the false color image immediately to its left. Thus, the top right panel shows the Newton diagram for collisions of NO in a molecular beam of 5% NO in Ar with Ar atoms in a neat Ar beam, and the bottom right panel shows the Newton diagram for collisions of NO in a beam of 5% NO in Ar with Ar atoms in a beam of 12% Ar in He. The scattering angle, θ, is measured clockwise from the center-of-mass frame initial NO velocity vector. Thus the zero-velocity intersection point of the two beams is near the bottom of the circle. On the circle of scattered $NO_{7.5}$ product in the top left panel of Figure 3, a very intense and sharp peak is observed near the bottom of the circle ($\theta \approx 90°$ in the center-of-mass-frame coordinate system.) This peak is at the origin of the laboratory frame and arises from $NO_{7.5}$ that has near-zero laboratory velocity. The scattering sphere for the higher-energy collisions shown in the bottom left panel is less intense, a result of the molecules scattering with greater velocity, and thus a larger and more diffuse scattering sphere. The NO molecular beam contains a small amount of $NO_{7.5}$ not cooled in the expansion, which is seen as a small diagonal band of intensity intersecting the circle of scattered $NO_{7.5}$ on the right side of both of the images near $\theta = 0°$.

Figure 4 shows two intensity profiles across the spike of intensity at $v'_{NO} = 0$ on the raw data. The velocity distribution in panel (a) corresponds to the top image in Figure 3, with collisions occurring between nitric oxide and argon in a molecular beam of neat argon.

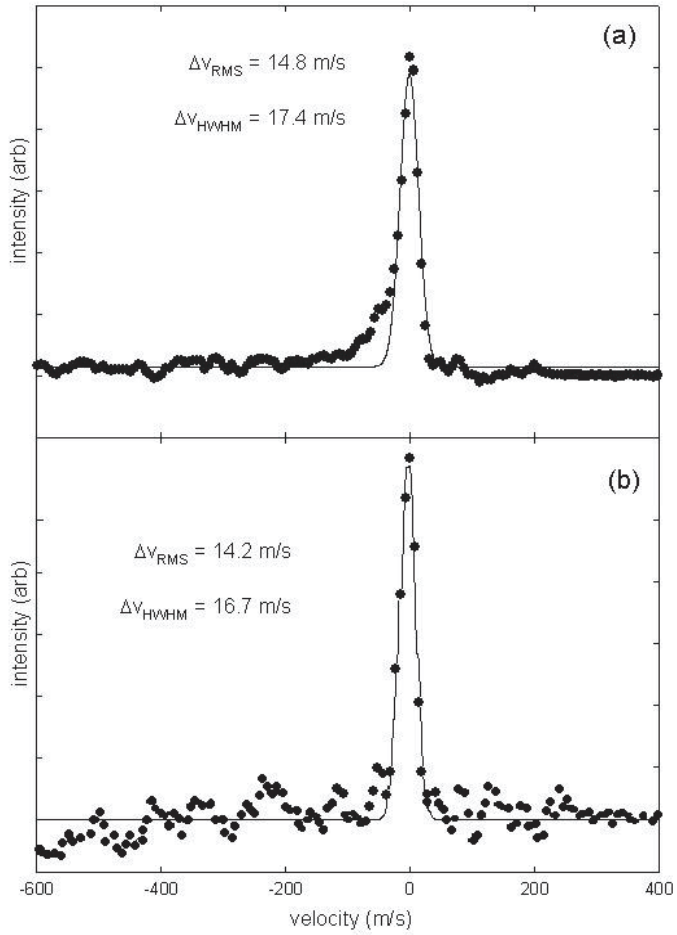

Fig. 4. The in-plane velocity distribution of NO($^2\Pi_{1/2}$, $j' = 7.5$) from the inelastic scattering NO($^2\Pi_{1/2}$, $j = 0.5$) + Ar $\rightarrow$ NO($^2\Pi_{1/2}$, $j' = 7.5$) + Ar. Panel (a) shows the velocity distribution for products resulting from collisions of NO molecules with Ar in a beam of neat Ar, and corresponds to the upper image in Figure 3. Panel (b) shows the velocity distribution for products resulting from collisions of NO molecules with Ar in a beam of 12% Ar seeded in He, and corresponds to the lower image in Figure 3. The data are fit to a symmetric distribution function, $f(v) = A\exp(-0.5v^2/b^2)$. Both curves are maximized at zero and (a) has a root-mean-square velocity of 14.8 m/s, and a hwhm velocity of 17.4 m/s. This corresponds to a temperature of ∼400 mK. The fit for (b) has a root-mean-square velocity of 14.2 m/s, and a hwhm velocity of 16.7 m/s. This corresponds to a temperature of ∼380 mK.

The velocity data is a two-dimensional projection of the three-dimensional distribution of scattered products, and there is no reason that the resulting velocity distribution should follow the statistics of a thermal equilibrium distribution. However, in order to assign a temperature to the distribution for the sake of comparing to other cooling techniques, we have chosen to fit the measured velocity profile to a one-dimensional Maxwell-Boltzmann form,

$$f(v) = \sqrt{\frac{m_{\mathrm{NO}}}{2\pi kT}} e^{-\frac{m_{\mathrm{NO}} v^2}{2kT}}, \qquad (1)$$

where k is the Boltzmann constant and T is temperature. The fit yields a temperature of 406 ± 28 mK, a root-mean-square (rms) velocity $(kT/m)^{1/2}$ of 14.8 ± 1.1 m/s, and a half-width at half-maximum velocity spread $[2\ \ln(2)\ kT/m]^{1/2}$ of 17.4 ± 1.2 m/s. For the purpose of comparison to the results of other researchers, it is useful to report the ratio of $E_{trans}(\mathrm{NO}_{7.5})$ to k, which we find experimentally to be 406 ± 28 mK.

Similarly, the intensity profile across the peak of intensity at the origin is shown in Figure 4b for the bottom image in Figure 3. A one-dimensional Maxwell-Boltzmann fit, described above, yields an rms velocity of 14.2 ± 1.1 m/s and a half-width at half-maximum velocity spread of 16.7 ± 1.2 m/s. This corresponds to a translational temperature of 391 ± 27 mK. Trapping and cooling NO molecules is feasible under these velocity and temperature conditions.

We have experimentally determined the density of the translationally cold NO molecules by a comparison of the absolute intensity at the origin in the images in Figure 3 with the image from a sample of thermal NO at known temperature and density. Our experimental density was found to be 10^8–10^9 molecules cm^{-3} at the lower collision energy and approximately one-fourth that for the higher collision energy. We believe that this density can be increased substantially by configuring an apparatus to optimize the reactant density in the scattering region. We are also configuring our apparatus to to produce greater densities of rotationally and translationally cold molecules. In particular, since lower rotational states are populated via collisions which cause forward scattering, cooling the molecular valve containing the molecular species of interest, nitric oxide, while simultaneously heating the valve containing the collision partner will increase the density NO(j') in the zero-velocity region. We have tested hot and cold valves and are currently making design improvements in order to have the ability to regulate the valve temperature.

4 Discussion

For our current results, molecular beam conditions were chosen to provide the velocity vector cancellation that results in scattered $\mathrm{NO}_{7.5}$ which is stationary in the laboratory frame of reference, or $\mathbf{v}'_{\mathrm{NO}}(j') = 0$. The conditions necessary for this cancellation may be derived from classical mechanics using vector algebra. The velocity cancellation occurs when the velocity of the system's center-of-mass is equal in magnitude and opposite in direction to the recoil velocity of the scattered $\mathrm{NO}_{7.5}$ molecule in the center-of-mass frame of reference. That is, when $\mathbf{u}'_{\mathrm{NO}} = -\mathbf{v}_{cm}$, where $\mathbf{u}'_{\mathrm{NO}}$ is the center-of-mass frame recoil velocity of the scattered $\mathrm{NO}_{7.5}$ and $\mathbf{v}_{cm}$ is the velocity of the NO + Ar center-of-mass in the laboratory-frame coordinate system. We have used the convention of primed variables to denote postcollision conditions and unprimed variables for the precollision conditions.

The velocity cancellation condition follows from the relation between the laboratory-frame velocity of the

scattered NO, $\mathbf{v'}_{\mathrm{NO}}$, and the center-of-mass frame velocity of the scattered $NO_{7.5}$: $\mathbf{u'}_{\mathrm{NO}} = \mathbf{v'}_{\mathrm{NO}} - \mathbf{v}_{cm}$. In order to simplify the algebra, we separate the vector cancellation condition into two scalar conditions for $\mathbf{u'}_{\mathrm{NO}}$, one for its magnitude and one for its direction. The former condition is most simply written as a constraint on velocity,

$$v_{cm} = -u'_{\mathrm{NO}}. \tag{2}$$

The recoil velocity of the NO molecule is equal in magnitude to the velocity of the system's center of mass. The postcollision energy of the NO molecule in the center-of-mass frame, E'_{rel}, is given by

$$E'_{rel} = \frac{1}{2}\mu\left(v'^{2}_{rel}\right) = \frac{1}{2}\mu\left(\left(\frac{M}{m_{\mathrm{Ar}}}\right)u'_{\mathrm{NO}}\right)^{2}. \tag{3}$$

The reduced mass is given by $\mu = m_{\mathrm{NO}}m_{\mathrm{Ar}}/M$, where m_{NO} and m_{Ar} are the masses of NO and Ar, and the total mass is $M = m_{\mathrm{NO}} + m_{\mathrm{Ar}}$. The zero-velocity constraint requires that $v_{cm} = u'_{\mathrm{NO}}$, so we have

$$E'_{rel} = \frac{1}{2}\mu\left(\left(\frac{M}{m_{\mathrm{Ar}}}\right)v_{cm}\right)^{2} = E_{cm}\left(\frac{m_{\mathrm{NO}}}{m_{\mathrm{Ar}}}\right). \tag{4}$$

The energy of the center-of-mass is the sum of the lab-frame energies of the NO and Ar minus the relative translational energy. The final rotational energy, E'_{rot}, of the scattered $NO_{7.5}$ molecules is equal to the difference between the initial and final relative energies. Thus, from equation (4) it follows that

$$E'_{rot} = \left(\frac{\mu}{m_{\mathrm{Ar}}}\right)E_{\mathrm{Ar}} + \left(\frac{\mu}{m_{\mathrm{NO}}}\right)E_{\mathrm{NO}} - \left(\frac{m_{\mathrm{NO}}}{m_{\mathrm{Ar}}}\right) \times \left(E_{\mathrm{NO}} + E_{\mathrm{Ar}} - \left(\frac{\mu}{m_{\mathrm{Ar}}}\right)E_{\mathrm{Ar}} - \left(\frac{\mu}{m_{\mathrm{NO}}}\right)E_{\mathrm{NO}}\right). \tag{5}$$

Substituting the energy terms with their definitions in terms of mass and velocity as given above, and solving for NO internal energy yields

$$E'_{rot}(\mathrm{NO}_{v'=0,j'}) = \left(1 - \frac{m_{\mathrm{NO}}}{m_{\mathrm{Ar}}}\right) \times E_{trans}(\mathrm{NO}_{v'=0,j=0.5}), \tag{6}$$

where $E_{trans}(\mathrm{NO}_{v'=0,\,j=0.5})$ is the lab-frame translational energy of the NO in the molecular beam. $E_{trans}(\mathrm{NO}_{v'=0,\,j=0.5})$ is the translational energy of the NO before collision and is the same as E_{NO} in equation (5). We expand the labels in equation (6) to emphasize the rotational energy transfer. $E'_{rot}(\mathrm{NO}_{v'=0,j'})$ is the amount of energy that must be deposited into the internal modes of the NO molecule in order to produce molecules that are stationary in the laboratory frame of reference. On inspection, it may seem surprising that only the energy of the NO and not that of Ar appears in this constraint. This is simply a direct algebraic consequence of the separation of the vector constraint into scalar constraints.

We now examine the latter constraint. The direction of the recoiling NO molecule can be determined starting with the Law of Cosines applied to velocities,

$$v^2_{\mathrm{NO}} = v^2_{cm} + u^2_{\mathrm{NO}} - 2u_{\mathrm{NO}}v_{cm}\cos(\theta_{cm}), \tag{7}$$

where θ_{cm} is the angle between the velocity of the center of mass and the precollision velocity of the NO molecular beam in the center-of-mass frame of reference. To derive an expression for the angular constraint, we begin by writing the velocity of the center of mass and the initial NO molecular beam velocity in the center-of-mass frame of reference, in terms of the lab-frame velocity of the NO molecules,

$$v^2_{cm} = \left(\frac{2E_{cm}}{M}\right) = \left(\frac{2}{M}\right) \times \left(\frac{m_{\mathrm{NO}}v^2_{\mathrm{NO}}}{2} + \frac{m_{\mathrm{Ar}}v^2_{\mathrm{Ar}}}{2} - \frac{\mu v^2_{\mathrm{NO}}}{2} - \frac{\mu v^2_{\mathrm{Ar}}}{2}\right), \tag{8}$$

and

$$u^2_{\mathrm{NO}} = \left[\left(\frac{m_{\mathrm{Ar}}}{M}\right)\sqrt{v^2_{\mathrm{NO}} + v^2_{\mathrm{Ar}}}\right]^2 = \frac{m_{\mathrm{Ar}}v^2_{\mathrm{NO}}}{M^2} + \frac{m_{\mathrm{Ar}}v^2_{\mathrm{Ar}}}{M^2}. \tag{9}$$

Solving equation (7) for $\cos(\theta_{cm})$ and substituting for the velocities defined in equations (8) and (9), it is seen that the condition for the scattering angle which must be met in order for the NO to have zero laboratory-frame velocity is:

$$\cos(\theta_{cm}) = \frac{E_{\mathrm{Ar}} - E_{\mathrm{NO}}}{\sqrt{\left(E_{\mathrm{NO}} + \frac{m_{\mathrm{NO}}}{m_{\mathrm{Ar}}}E_{\mathrm{Ar}}\right)\left(E_{\mathrm{NO}} + \frac{m_{\mathrm{Ar}}}{m_{\mathrm{NO}}}E_{\mathrm{Ar}}\right)}}, \tag{10}$$

where E_{NO} and E_{Ar} are the kinetic energies of NO and Ar, respectively. Since the angular distribution of the inelastically scattered $NO_{7.5}$ is rather broad, this condition is easy to establish, and is indeed established for our experimental conditions. More generally, the translational energy of the NO beam can be selected in order to ensure that the required $|\mathbf{u'}_{\mathrm{NO}}|$ corresponds to the energy an NO rotational quantum state, and the translational energy of the Ar beam can be selected to ensure that sufficient scattering events satisfy the angular condition.

Equation (6) has a remarkable consequence for the scattering of partners with identical masses (ND_3 colliding with Ne, for instance). The internal energy, $E'_{\mathrm{int}}(\mathrm{NO}_{v'=0})$, for scattered molecules satisfying the zero-velocity condition is zero. Thus, for molecules colliding with scattering partners of equal mass, the molecules that satisfy the condition of $v_{cm} = -u'_{\mathrm{NO}}$ are those that scatter elastically. Under this condition the velocity spread, for those molecules that scatter back toward their point of collision, is exactly zero, since all elastic scattering products must lie on a Newton sphere that intersects the origin, regardless of collision energy. Those scattered in the appropriate direction, $v_{cm} = -u'_{\mathrm{NO}}$, will be completely stationary in the laboratory, and a collision energy can be chosen to optimize scattering amplitude in that direction.

Our NO molecular beam has a translational energy of 5.26 ± 0.21 kJ/mol. For this translational energy equation (6) states that an internal energy in the NO of 1.32 ± 0.05 kJ/mol is required for an NO molecule to become stationary upon colliding with an Ar atom. The rotational energy of NO in the $j' = 7.5$ quantum state is 1.297 kJ/mol. Since the energy spread in the NO beam is larger than the energy difference, $NO_{7.5}$ molecules that are scattered in the correct direction, given by equation (10) above, will be nearly stationary in the laboratory frame. For scattering between NO and Ar in the neat Ar beam, the initial relative collision energy is 5.65 ± 0.36 kJ/mol; if 1.297 kJ/mol is taken up by rotation of the $NO_{7.5}$ molecule then ∼4.35 kJ/mol remains for translational energy of the recoiling partners in the center-of-mass frame. We can check this by measuring the radius of the scattering ring in Figure 3. We measure a translational energy of the recoiling $NO_{7.5}$ to be 2.46 ± 0.13 kJ/mol. This corresponds to an NO + Ar recoil energy of 4.31 ± 0.13 kJ/mol, in agreement with expected value. For scattering between NO and Ar in the 12% Ar beam, the initial relative collision energy is 14.7 ± 0.9 kJ/mol. Again, 1.297 kJ/mol is taken up by rotation of the scattered $NO_{7.5}$ molecules, thus 13.4 ± 0.9 kJ/mol remains for translation in the recoiling collision partners. Experimentally this is seen to be true for the image in Figure 6, since the radius for the scattering ring corresponds to an NO + Ar recoil energy of 13.7 ± 0.6 kJ/mol.

We can predict the distribution in the laboratory-frame velocity of the translationally cold NO from the spread in the velocities of the NO and Ar beams. Ours is a simple analysis of the behavior of $\mathbf{v}'_{\mathrm{NO}} = \mathbf{u}'_{\mathrm{NO}} + \mathbf{v}_{cm}$ around $\mathbf{u}'_{\mathrm{NO}} = -\mathbf{v}_{cm}$ that characterizes the cold molecules. The center-of-mass energy is the sum of the mass-weighted energies of argon and nitric oxide

$$E_{cm} = \frac{m_{\mathrm{Ar}}}{M}E_{\mathrm{Ar}} + \frac{m_{\mathrm{NO}}}{M}E_{\mathrm{NO}} = \frac{1}{M}\left(m_{\mathrm{Ar}}E_{\mathrm{Ar}} + m_{\mathrm{NO}}E_{\mathrm{NO}}\right). \tag{11}$$

Solving for the square of the velocity of the center of mass, we have

$$v_{cm}^2 = \frac{2}{M}\left(\frac{m_{\mathrm{Ar}}}{M}E_{\mathrm{Ar}} + \frac{m_{\mathrm{NO}}}{M}E_{\mathrm{NO}}\right) = \frac{m_{\mathrm{Ar}}^2}{M^2}v_{\mathrm{Ar}}^2 + \frac{m_{\mathrm{NO}}^2}{M^2}v_{\mathrm{NO}}^2. \tag{12}$$

The postcollision translational energy of NO follows from equation (1) and is given by

$$E'_{\mathrm{NO}} = \frac{m_{\mathrm{Ar}}}{M}E'_{rel} = \frac{m_{\mathrm{Ar}}}{M}\left(E_{rel} - E'_{\mathrm{int}}\right). \tag{13}$$

Solving for the square of the final center-of-mass velocity of the recoiling NO, we have

$$u'^2_{\mathrm{NO}} = \frac{2}{m_{\mathrm{NO}}}\left(\frac{m_{\mathrm{Ar}}}{M}E'_{rel}\right) = \frac{m_{\mathrm{Ar}}^2}{M^2}v_{\mathrm{Ar}}^2 + \frac{m_{\mathrm{Ar}}^2}{M^2}v_{\mathrm{NO}}^2 - \frac{2m_{\mathrm{Ar}}}{m_{\mathrm{NO}}M}E'_{\mathrm{int}}. \tag{14}$$

The resonance condition is $u'_{\mathrm{NO}} = v_{cm}$, or $v'_{\mathrm{NO}} = u'_{\mathrm{NO}} - v_{cm}$. In the vicinity of the resonance condition, it can be shown that

$$\frac{\partial(v'_{\mathrm{NO}})}{\partial v_{\mathrm{Ar}}} = \frac{\partial(u'_{\mathrm{NO}} - v_{cm})}{\partial v_{\mathrm{Ar}}} = \frac{\partial u'_{\mathrm{NO}}}{\partial v_{\mathrm{Ar}}} - \frac{\partial v_{cm}}{\partial v_{\mathrm{Ar}}} = 0 \tag{15}$$

and

$$\frac{\partial(v'_{\mathrm{NO}})}{\partial v_{\mathrm{NO}}} = \frac{\partial(u'_{\mathrm{NO}} - v_{cm})}{\partial v_{\mathrm{NO}}} = \frac{\partial u'_{\mathrm{NO}}}{\partial v_{\mathrm{NO}}} - \frac{\partial v_{cm}}{\partial v_{\mathrm{NO}}} = \frac{v_{\mathrm{NO}}}{v_{cm}}\left(\frac{m_{\mathrm{Ar}}^2 - m_{\mathrm{NO}}^2}{M^2}\right). \tag{16}$$

For finite differences in the scattering velocity of NO, we have a relationship between the postcollision velocity spread, $\Delta v'_{\mathrm{NO}}$, and the velocity spread in the NO molecules before collision:

$$\Delta v'_{\mathrm{NO}} = \left(\frac{v_{\mathrm{NO}}}{v_{cm}}\right)\left(\frac{m_{\mathrm{Ar}}^2 - m_{\mathrm{NO}}^2}{(m_{\mathrm{Ar}} + m_{\mathrm{NO}})^2}\right)\Delta v_{\mathrm{NO}}. \tag{17}$$

To first order the spread in v'_{NO} does not depend on the spread in v_{Ar}, as equation (6) indicates, but only on v_{NO}. The dependence on the spread in v_{NO} is interesting as it shows a kinematic compression of the velocity spread.

For collisions between 5% NO in Ar colliding with neat argon, $\Delta v'_{\mathrm{NO}} = 0.21\Delta v_{\mathrm{NO}}$, and for collisions between 5% NO in Ar colliding with argon seeded in helium, $\Delta v'_{\mathrm{NO}} = 0.12\Delta v_{\mathrm{NO}}$, even colder for higher collision energy! As discussed above, our NO beam has a velocity spread (hwhm) of 27 m/s, so the distribution of v'_{NO} around $v'_{\mathrm{NO}} = 0$ has a predicted width (hwhm) of only 4.4 m/s for NO collisions with neat argon, and a predicted width of 2.4 m/s for NO collisions with argon seeded in helium. These values represent the limit on the temperature of our cold NO that can be achieved with our current NO beam source, and gives $T = E_{trans}/k = 34.9$ mK for NO colliding with the neat Ar beam and 10.4 mK for the higher collision energy system. This compression is the reason that even with the broadening due to ion imaging detection of the scattered NO we see a v'_{NO} distribution that is substantially narrower than the velocity spread in the NO beam itself. This is a result of the cancellation of the variation in v_{NO} due to its similar influence on both u'_{NO} and v_{cm}, just as the cancellation of u'_{NO} and v_{cm} leads to a most probable v'_{NO} of zero. Specifically, it can be seen from equation (17) that $\Delta v'_{\mathrm{NO}}$ is inversely proportional to v_{cm}, which varies with v_{Ar}.

Our NO may indeed be this cold, but our apparatus does not allow us to resolve NO velocities associated with such a low temperature. Production of NO beams with narrower velocity spreads is possible, so this limit can be reduced. As noted earlier during the discussion of equation (6), for molecular collisions in which the masses of the two particles are equal, our first-order approximation shows that the contribution of the spread in both beam velocities to the velocity distribution of the scattered molecules disappears.

The measured RMS velocity spreads, 14.8 m/s and 14.2 m/s, are more than three times that predicted by equation (17) for the lower collision energy, and more than

six times that predicted for the higher collision energy. Our measured velocity spread of cold NO molecules is an upper limit to the actual spread in velocities, as is the temperature associated with this velocity spread. In our experiment there are several sources that broaden the reported velocity distribution. First is the resolution of the microchannel plate detector and camera, about 8 m/s. A higher-resolution detection system would potentially yield a narrower distribution. Second, the resolution of the velocity mapping itself can be compromised by charge repulsion of the ions and imperfect ion optics. From measurement of parent ions in our molecular beams we estimate this may add approximately 10 m/s of velocity spread. Third is the velocity imparted to the detected NO^+ ions by the recoil of the electron from the NO upon two-photon ionization. The recoiling photoelectron imposes a velocity spread of approximately 10 m/s. We can minimize this effect with a longer-wavelength ionization photon. A fourth source of broadening comes from the nature of the measurement, which is a projection of the three-dimensional spherical velocity distribution onto the two-dimensional detector. Scattering above and below the scattering plane gives rise to the asymmetric tail on the distribution of Figures 5 and 7. These sources of broadening associated with detecting the cold NO via ion imaging are considerably greater that the expected velocity spread of the cold NO. Improvements in non-perturbative detection will reduce these sources of broadening in order to determine more accurately the NO translational energy.

5 Concluding remarks

The technique of crossed molecular beam scattering to produce cold molecules has the potential to produce significant numbers of translationally cold molecules in a specific quantum state of our choosing. The generality and ease of application of this technique makes it well suited for sub-kelvin cooling of molecules, as its operation does not depend on any particular physical property of the molecular species. The vector constraint that must be satisfied to produce zero-velocity molecules, $\mathbf{u'}_{\mathrm{NO}} = -\mathbf{v}_{cm}$, can readily be met. This represents two independent scalar constraints in a system in which (for fixed 90° molecular beam intersection angle) there are three experimental variables — the kinetic energies of the two colliding molecules and the ratio of their masses — whose values can be selected to achieve the zero-velocity condition. For producing zero-velocity species AB the AB energy can be adjusted by changing the temperature of the AB free-jet expansion nozzle, and the diluent gas in which it is seeded. The energy of the collider species can be selected by the temperature of its free-jet expansion nozzle, as has been mentioned, and since the chemical identity of the collider species is not important, the ratio of the masses can be readily selected.

The authors would like to express their gratitude to Mark Jaska and Bradley F. Parsons for the considerable assistance they provided during the course of this research. Funding for this work was provided by the U.S. Department of Energy, Office of Basic Energy Science, Division of Chemical Sciences, Geosciences, and Biosciences. Sandia is a multiprogram laboratory operated by Sandia Corporation, a Lockheed Martin Company, for the United States Department of Energy's National Nuclear Security Administration under contract DE-AC04-94AL85000.

References

1. C.E. Weiman, D.E. Pritchard, D.J. Wineland, Rev. Mod. Phys. **71**, S253 (1999)
2. M.H. Anderson, J.R. Ensher, M.R. Matthews, C.E. Wieman, E.A. Cornell, Science **269**, 198 (1995)
3. C.C. Bradley, C.A. Sackett, J.J. Tollett, R.G. Hulet, Phys. Rev. Lett. **75**, 1687 (1995)
4. K.B. Davis, M.O. Mewes, M.R. Andrews, N.J. van Druten, D.S. Durfee, D.M. Kurn, W. Ketterle, Phys. Rev. Lett. **75**, 3969 (1995)
5. S.L. Rolston, W.D. Phillips, Nature **416**, 219 (2002)
6. K. Burnett, P.S. Julienne, P.D. Lett, E. Tiesinga, C.J. Williams, Nature **416**, 225 (2002)
7. S.A. Diddams, T. Udem, J.C. Bergquist, E.A. Curtis, R.E. Drullinger, L. Hollberg, W.M. Itano, W.D. Lee, C.W. Oates, K.R. Vogel, D.J. Wineland, Science **293**, 825 (2001)
8. A. Kerman, V. Vuletic, C. Chin, S. Chu, Phys. Rev. Lett. **84**, 439 (2000)
9. C. Monroe, W. Swann, H. Robinson, C. Wieman, Phys. Rev. Lett. **65**, 1571 (1990)
10. W. Ketterle, Int. J. Mod. Phys. **16**, 4537 (2002)
11. H.L. Bethlem, G. Meijer, Int. Rev. Phys. Chem. **22**, 73 (2003)
12. F. Masnou-Seeuws, P. Pillet, Adv. At. Mol. Opt. Phys. **47**, 52 (2001)
13. J.T. Bahns, P.L. Gould, W.C. Stwalley, Adv. At. Mol. Opt. Phys. **42**, 171 (2000)
14. J.P. Shaffer, W. Chalupczak, N.P. Bigelow, Phys. Rev. A **63**, 021401 (2001)
15. H.R. Thorsheim, J. Weiner, P.S. Julienne, Phys. Rev. Lett. **58**, 2420 (1987)
16. T. Takekoshi, B.M. Patterson, R.J. Knize, Phys. Rev. Lett. **81**, 5105 (1998)
17. N. Vanhaecke, W. de Souza Melo, B. Laburthe Tolra, D. Comparat, P. Pillet, Phys. Rev. Lett. **89**, 063001 (2002)
18. E.A. Donley, N.R. Clausen, S.T. Thompson, C.E. Weiman, Nature **417**, 529 (2002)
19. C.A. Regal, C. Ticknor, J.L. Bohn, D.S. Jin, Nature **424**, 47 (2003)
20. J.D. Weinstein, R. deCarvalho, T. Guillet, R. Friedrich, J.M. Doyle, Nature **395**, 148 (1998)
21. J. Kim, B. Friedrich, D.P. Katz, D. Patterson, J.D. Weinstein, R. DeCarvalho, J.M. Doyle, Phys. Rev. Lett. **78**, 3665 (1997)
22. H.L. Bethlem, G. Berden, F.M.H. Crompvoets, R.T. Jongma, A.J.A. van Roij, G. Meijer, Nature **406**, 491 (2000)
23. H.L. Bethlem, G. Berden, A.J.A. van Roij, F.M.H. Crompvoets, G. Meijer, Phys. Rev. Lett. **84**, 5744 (2000)
24. M. Gupta, D. Herschbach, J. Phys. Chem. A **103**, 10670 (1999)

25. M.S. Elioff, J.J. Valentini, D.W. Chandler, Science **302**, 1940 (2003)
26. K.T. Lorenz, M.S. Westley, D.W. Chandler, Phys. Chem. Chem. Phys. **2**, 481 (2000)
27. M.S. Elioff, D.W. Chandler, J. Chem. Phys. **117**, 6455 (2002)
28. D.W. Chandler, D.H. Parker, in *Advances in Photochemistry*, edited by D.C. Neckers, D.H. Volman (Wiley, New York, 1999), Vol. 25
29. D.H. Parker, A.T.J.B. Eppink, J. Chem. Phys. **107**, 2357 (1997)
30. A.T.J.B. Eppink, D.H. Parker, Rev. Sci. Instrum. **68**, 3477 (1997)
31. J. Luque, D.R. Crosley, LIFBASE: Database and Simulation Program (v 1.6), SRI International Report No. MP 99-009, 1999
32. K.T. Lorenz, M.S. Westley, D.W. Chandler, in *ACS Symposium Series 770: Imaging in Chemical Dynamics*, edited by A.G. Suits, R.E. Continetti (American Chemical Society, Washington, DC, 2001)
33. *Atomic and Molecular Beam Methods*, edited by G. Scoles (Oxford University Press, New York, 1988), Vol. 1
34. M.H. Alexander, D.E. Manolopoulos, H.J. Werner, B. Follmeg, HIBRIDON, VER. 4.1, University of Maryland at College Park, MD, 2001